Defects Induced Ferromagnetism in Mg-doped ZnO Nanoparticles

A thesis submitted
in partial fulfillment of requirement for
the award of degree of

Masters of Technology
in
Materials Science and Engineering

Submitted by
Pritampal Singh Gill
Reg. No. 601202009

Under the guidance of
Dr. N.K.Verma
Senior Professor

School of Physics and Materials Science
Thapar University
(Established under section 3 of UGC Act, 1956)
Patiala -147001, India

July 2014

ACKNOWLEDGEMENT

In pursuit of this academic endeavor I feel that I have been especially fortunate as inspiration, guidance, direction, co-operation, love and care all came in my way in abundance and it seems almost an impossible task for me to acknowledge the same in adequate terms.

I express my sincere thanks to my supervisor, to Dr. N. K. Verma, *Senior Professor, School of Physics and Materials Science, Thapar University, Patiala*, for his esteemed supervision, incessant support, inspiration and constructive criticism throughout my research work.

I accord my thanks to Dr. Kulvir Singh, *Professor and Head, School of Physics and Materials Science, Thapar University, Patiala,* for providing me with the opportunity to conduct this work and bring it out in the present form.

I offer special thanks and regards to Mr. Jaspal Singh, Ms. Gitanjali Dhir, Ms. Lavanya Khanna, Mrs. Kamaldeep Kaur and Ms. Iman, Research Scholars, School of Physics and Materials Science, Thapar University, Patiala, for providing immense support in performing, characterizing and evaluating the thesis work.

I would also like to thank my friends (Gaganjot Singh, Bharat Bhushan, Gaurav Kalia, Kirpal Singh) for helping me throughout my degree.

Finally, I would also express my sincere gratitude to my parents, for their encouragement and moral support, which always inspired me and stood by me as strong pillars.

Pritampal Singh Gil

Reg. No. 601202009

CERTIFICATE

This is to certify that report entitled **"Defects induced ferromagnetism in Mg-doped ZnO nanoparticles"** submitted by Pritampal Singh Gill, Roll No. 601202009, student of M. Tech, Thapar University, Patiala, was carried out by him under my supervision. He has not submitted this material for the credit towards any other degree at Thapar University, Patiala or at any other University.

Dr. N.K. Verma
Senior Professor
School of Physics and Materials Science
Thapar University, Patiala

(Countersigned by)

Kulvir Singh
Professor & Head
School of Physics and Materials Science
Thapar University, Patiala

S.K. Mohapatra
Dean of Academic Affairs
Thapar University, Patiala

iii

ABSTRACT

$Zn_{1-x}Mg_xO$ (x = 0, 5, 10, 15, 20) nanoparticles were successfully synthesized using sol-gel method. Structural analysis has been found to reveal that synthesized nanoparticles characterize wurtzite phase having hexagonal structure. Crystallite size calculated using Debye-Scherer equation has indicated a decrease in crystallite size from 20 to 11 nm. The peak shifting towards higher diffraction angle with increasing Mg-doping concentration has confirmed Mg-substitution. Morphological analysis has been found to reveal almost spherical morphology with average particle size 15 nm for 10% Mg-doped ZnO nanoparticles. Clear lattice fringes and sharp diffraction rings observed from HRTEM and SAED patterns, respectively, also revealed formation of well crystallized nanoparticles. EDS patterns has showed the successful doping of Mg in ZnO lattice without formation of any impurity phases. PL spectra revealed blue-shift in band gap with increasing Mg-doping concentration and the reason has been attributed to the wider band gap of MgO (7.3 eV) in comparison to ZnO (3.17 eV). The decreasing ESR signal with increasing Mg-doping concentration has clearly indicated the decreasing oxygen vacancy/defects. All the synthesized nanoparticles have been found to display room temperature ferromagnetism. Increasing Mg-doping concentration has resulted in decaying saturation magnetization value. The reason has been ascribed to decreasing oxygen vacancy/defects with increasing Mg-doping as revealed by ESR.

LIST OF FIGURES

LIST OF TABLES

Contents

Chapter-1

Chapter-1

Introduction

1.1 Introduction

Nanoscience and nanotechnology deal with small-sized structures or materials. A nanometer (nm) is one billionth of a meter, or $l0^{-9}$ m. Nanoscience is a combination of two words, nano meaning "dwarf" and the word science. It deals with the science of materials and technologies in the scale range of 1-100 nm [1, 2]. This means that nanoscience deals with a few hundred to a few thousand atoms or atomic clusters. Nanostructured materials are those with at least one dimension falls in nanometer scale, and include nanoparticles (including quantum dots, when exhibiting quantum effects), nanorods and nanowires, thin films, and bulk materials made of nanoscale building blocks or consisting of nanoscale structures. The physical properties in the micrometer scale mostly exhibit in same form same as that of bulk. Whereas the at nanoscale they exhibit physical properties, which are different from that of bulk. Properties not seen on a macroscopic scale are now becoming important on nanoscale such as quantum mechanics, optics, magnetism, surface reactivity and thermodynamics.

Nanotechnology is the practical aspect of nanoscience [3, 4].Nanoscience is used to describe the interdisciplinary fields of science devoted to the study of nanoscale phenomena employed in nanotechnology.

1.2 History

The term nanotechnology was coined in1974 by Norio Taniguchi, professor at Tokyo Science University who pointed out the trend of precision manufacturing at the scale of nanometers [5]. With nanotechnology being hailed as the science of future and the technology of the next generation, respectively along with their infinite market potential, the key focus lies on the control, manipulation and construction of matter at the atomic and molecular level

1.3 Properties of Nanomaterials

Nanomaterials possess different and unique properties as compared to their bulk counterpart. The properties of nanomaterials include increased strength, enhanced diffusivity, reduced density, higher electrical resistance, lower thermal conductivity, higher absorption etc. in comparison with conventional coarse grained materials.

Amongst the nano and bulk scale the properties exhibited by them are entirely different and this feature characterizes them. A lot of research has been carried out in order to investigate these properties and also to understand their fundamentals. The reasons of existing physical properties of nanomaterials are generally related to different origins such as high surface to volume ratio, high surface energy, quantum confinement, reduction in imperfections etc.

(1) Due to huge amount of atoms present at the surface in the nanomaterials, they are highly reactive and hence, accordingly possess considerably lower melting point or phase transition temperature and also, significantly compact lattice constants.

(2) Mechanical properties of nanomaterials are one or two orders of magnitude higher than that their bulk counterpart. This remarkable enhancement in mechanical strength is attributed to reduction in the probability of defects at nanoscale.

(3) Optical properties at nanoscale are entirely different from that of its bulk counterpart. The optical absorption peak of a semiconductor nanoparticle shifts to a short wavelength, owing to the increase in band gap. This results in variation in the color of metallic nanoparticles with the changing size due to the phenomena known as surface plasmon resonance.

(4) A decrease in electrical conductivity of nanomaterials with reducing dimensions to nano scale is owed to increasing surface scattering whereas it has also been found to improve appreciably, due to the better ordering in microstructures, such as in polymeric fibrils.

(5) Magnetic properties of nanostructured materials are noticeably different from that of their bulk counterpart. Ferromagnetic behavior in bulk materials transfers to superparamagnetism at the nanometer scale owing to the huge surface energy.

(6) An intrinsic thermodynamic property of nanostructures and nanomaterials is self-purification. Heat treatment results in increasing the diffusion of impurities and intrinsic structural defects dislocations.

So, all these properties are size dependent. In other words, properties of nanostructured materials

can be tuned considerably by varying the shape, size or extent of agglomeration.

1.4 Dilute Magnetic Semiconductors

The material joining both the characteristics of semiconductor and magnetic material are known as Dilute Magnetic Semiconductors (DMS) [6]. The DMS are semiconducting materials in which the fraction of host cations are substituted by magnetic ions (Fe, Co, Ni etc) or appropriate rare earth elements as shown in Fig1.1.

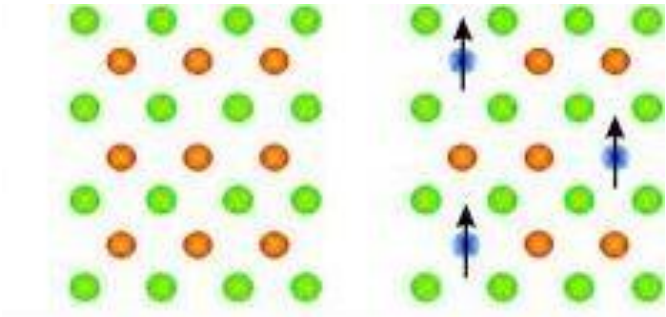

Figure1.1 Semiconductor host (parrot) atoms with magnetic impurity in (blue)

Mass storage of information crucial for information technology is carried out by magnetic recording (hard disks, magnetic disks) using electronic spins in ferromagnetic materials. It is then quite expected that both the charge and spin of electrons can be used at the same time to enhance the performance of devices. This is the base of the field of spintronics, which can be exploited in future for the solution to reduce the size of existing microelectronic devices. In order to realize functional spintronic devices materials with ferromagnetic ordering at room temperature are required. DMS being ferromagnetic semiconductors are the best for this need.

DMS possess both properties namely, semi-conducting and ferromagnetism. So, these properties can possibly result in influencing the charge as well as spin of the electron at the same time. Hence, this opens a new field in semiconducting technology to discover new electronic devices. One such example of its application can be insertion of DMS materials into magnetic metal and semiconductor so as to realize expulsion of carriers with spin polarization into non-magnetic semiconductor, and this can be exploited for creating spin polarized light-emitting diode [7]**.** Moreover, it is understandable that the origin of the ferromagnetism observed in some DMS,

such as $Ga_{1-x}Mn_xAs$, is due to s, p–d exchange interaction. Therefore the confirmation of s, p–d exchange interaction is the most important task to be carried out when new materials intended to be DMS are synthesized [8,9].

1.4.1 Selection of DMS materials

Two major criteria are considered to select the most promising materials for semiconductor spintronics are given as follows:

- Ferromagnetic behavior at room temperature.
- A major advantage would be there if an already existing technology becomes base for the material in other applications.

1.4.2 Physical Properties

1.4.2.1 Exchange interaction

When magnetic ions are substitutionally doped into semiconductors this results spin-spin exchange interaction with carriers, which further will lead to interesting effects such as anomalous Hall Effect, giant Geeman splitting and room temperature ferromagnetism. The spin-spin exchange interactions are considered as the key interactions through which DMS materials differ from non-magnetic materials. In DMS, exchange interactions between s electrons in conduction band, p electrons in valence band and d electrons of magnetic ions are known as sp-d exchange interaction and d electrons of magnetic ions are known as d-d exchange interaction) [10].

1.4.2. 2 Magnetotransport properties

- Negative Magnetoresistance: In this case, with increase in external field, BMP will be destroyed more and more, thus lead to more and more leased carriers to conduct. Thus, DMS will demonstrate a negative magneto resistance at low temperature.
- Enhanced Magnetophotonic Effect: It is another unique property of DMS, change of polarization plane (Faraday angle) can display magnitude of interactions between s, p and d electrons.

1.4.3 Zeeman Effect

When a magnetic field is applied to semiconductor, the energy of electrons and holes with their spin magnetic moments parallel to the field is lowered. In DMS, the ions become magnetized in the presence of an applied magnetic field. Thus, in addition to the external field, the electrons and holes feel a large magnetization from the ions. This results in Zeeman effect that can be hundreds of times larger in DMS materials than in non magnetic semiconductor. This in turn results in a giant faraday rotation which means that DMS have potential applications as magneto optic materials with large magneto optic coefficients.

1.5 Literature Review

The literature has been reviewed in detail to get full insight of the research work.

Sieber et al. [11] in 1998 deposited ZnO: Al films (1.1, 2.4, 4.4, 5.6 and 8.6 at. % Al) by reactive co-sputtering technique on silicon substrates. The structural analysis was carried out using FE-SEM and HREM. The films Al-doped (5 at. %) were found to possess columnar structure of hexagonal wurtzite type. Al influences the growth of nuclei of columnar grains. Near to interface, nanocrystallites of different phases were found. At the ZnO/Si interface an amorphous silicon oxide layer was formed. The results showed that nanocrystalline region grows with increasing Al-doping. At all concentrations above 5 at.% the films exhibit a nanocrystalline structure. An amorphous silicon oxide layer was found at the interface

Ma et al. [12] in 2008 deposited Zn, Al, Pt, Ag, and Au nonmagnetic metallic films on the surface of ZnO film by high vacuum annealing at different temperatures. Magnetic study showed that Zn, Al, Pt/ZnO films displayed room temperature ferromagnetism (RTF) after the vacuum annealing, while Ag, Au/ZnO films did not. Results from TEM and XPS showed that this RTF was due to the unique structure of metal clusters and also, the interaction of metal clusters and ZnO matrix. RTF disappeared in Al/ZnO after a subsequent annealing in air as, metal clusters were oxidized. Pt/ZnO remained ferromagnetic, as the metal cluster structure was stable subjected to the air annealing.

Qiu et al. [13] in 2008 synthesized $Zn_{1-x}Mg_xO$ ($0 \leq x \leq 0.10$) nanoparticles by a novel rheological phase reaction route. XRD study revealed the wurtzite structure formation for ZnO. However, on

increasing dopant concentration beyond x = 0.15, secondary phase (MgO) was observed. Thereby, this indicated the solubility limit to be x = 0.15. SEM micrographs reveal no change in particle size and morphology with Mg-doping in ZnO. Experimental and theoretical investigations of photocatalysis were carried out. All $Zn_{1-x}Mg_xO$ samples were found to exhibit high photoactivities. However, it first increased with the Mg doing content up to x = 0.05, and then decreased with further doping of Mg to x = 0.10. Density function theory calculations pointed towards the largely affected conduction band with Mg- doping, but no such effects on the valence band. The enhanced photocatalytic activities were attributed to shifting of the conduction band toward higher energies. Whereas, the reduced the photocatalytic activities were a result of the incorporation of Mg ions at interstitial sites which lead to the impurity levels and acted as the trapping or recombination centers for the photoinduced electrons and holes.

Chawla et al. **[14] in 2009** prepared Li-doped ZnO (2–15 at. %) nanorods by solid state reaction method. All the synthesized nanorods were found to possess hexagonal wurtzite structure. Li-doping resulted in increase in lattice parameters thereby, indicating its uniform doping. SEM revealed best rod formation for 2% Li-doped ZnO. Undoped ZnO exhibited diamagnetism. 2% Li-doped ZnO displayed ferromagnetism.

Chawla et al. [15] in 2009 synthesized nanocrystalline powder of ZnO doped with Li/Na by solid state reaction method that exhibits ferromagnetism up to 554 K which was confirmed from magnetic hysteresis, where substitutional Li^+ /Na^+ in cation site induced local magnetic moments on oxygen atoms. High Curie temperature in the material was due to optimum dopant concentrations which enables ferromagnetic exchange interaction. This concludes that observed RTFM (Room Temperature Ferromagnetism) is an intrinsic property of ZnO:Li and ZnO:Na nanocrystals which was due to formation of magnetic domains. Alkali ion doping induces intrinsic FM (Ferromagnetism) in ZnO. Thus alkali doped ZnO could prove to be a better DMS material compared to transition metal ions. Such novel DMS based on a multifunctional material such as ZnO could alter the way for a new class of magneto optic and spintronic material for variety of applications.

Gao et al. [16] in 2010 prepared $Zn_{1-x}Al_xO$ () nanoparticles using sol-gel method. XRD showed that $Zn_{1-x}Al_xO$ nanoparticles formed wurtzite structure thereby, indicating that Al atoms successfully substituted Zn atoms in the ZnO lattice without formation of extra phases. Ferromagnetism was exhibited by all the synthesized nanoparticles. The observed magnetism

was attributed to doping-induced oxygen vacancies indicated by Raman, PL and XPS analysis. The study suggests that creation of oxygen vacancies is an effective way to induce ferromagnetism.

Zhuang et al. [17] in 2010 synthesized ZnO nanowires doped with Mg on Au-coated Si substrates via chemical vapor deposition method. The structural, compositional, morphological and optical properties of the samples were characterized by XRD, SEM, TEM and PL spectroscopy. The nanowires were found to be single crystalline in nature and also, they possessed preferential growth direction along [0001]. This shows that the introduction of divalent Mg ion in the ZnO lattice does not affect the direction of growth. TEM revealed that ZnO nanowires had average diameter and length of about 60 nm and several hundred micrometers, respectively. The PL spectroscopy indicated a blue shift from the bulk band gap emission. The reason may be attributed to the Mg doping in ZnO.

Karthikeyan et al. [18] in 2010 synthesized Mg-doped ZnO nanostructures with sol–gel method. XRD patterns showed that the ZnO nanostructures characterize wurtzite structure and also revealed that compression in lattice parameters takes place with Mg-substitution. In optical absorption spectra, exciton absorption peak was observed at 372 nm and doping led to blue shift due to the Burstein–Moss effect and change in particle size. Photoluminescence measurements show strong peaks at around 385, 394 nm due to band edge exciton emission while peaks at 469 and 558 were attributed to oxygen ion vacancy and formation of Vo^{+} and Vo^{++} centers in nanostructures.

Park et al. [19] in 2010 reported room-temperature ferromagnetism (RTF) in C-doped ZnO. The theoretical explanations of RTF in ZnO:C are based on the incorporation of C at the O site and on the p-p exchange interaction between the localized C_{2p} spins and valence band holes. Contrary to the theoretical explanations, all the C-doped ZnO films exhibited n-type conductivity. Furthermore, most of the carbons were not incorporated at the O site, but rather at the interstitial or Zn site, or formed C clusters. Although there may exist a growth method that can lead to incorporation of C at O site, our experimental results indicate that the defect-induced ferromagnetism mechanism can better explain most of the observed RTF in the PLD-grown ZnO:C films.

Singh et al. [20] in 2011 prepared Mg doped zinc oxide ($Mg_xZn_{1-x}O$, x = 0, 5, 10 and 20 at. %) nanowires by two step process. Firstly, ZnO powder was prepared using a simple thermal

oxidation and then, doping of Mg was done by solid state diffusion. XRD data reveals the formation of wurtzite structure of the synthesized nanowires. Also, a continuous decrease in the lattice parameter was observed (in particular, the c-axis parameter) with increasing Mg-content The hydrogen absorption measurements at room temperature reveals that hydrogen storage capacity first increases with Mg-doping upto 10 at.%. However, on further increase in Mg-content, the capacity decreases

Viswanatha et al. [21] in 2012 synthesized Mg-doped ZnO nanoparticles successfully with precipitation method having diameters ranging from 50 to 100 nm. The presence of Mg was confirmed by infrared spectroscopic IR studies. The morphological analysis of synthesized material carried out with SEM shows the granular shaped and well dispersed ZnO nanoparticle while the Mg-doped ZnO nanoparticles possessed flake like structures. The elemental analysis by EDAX indicated presence of zinc, oxygen and magnesium without any other traces. The average crystallite size (using Debye-Scherrer equation) of ZnO and Mg-doped ZnO nanoparticles was found to be 86 and 59 nm respectively. The optical band gap of doped and undoped was studied. It was found that the band gap reduced due to Mg doping in lattice.

Viswanatha et al. [22] in 2012 prepared ZnO and Mg-doped ZnO nanoparticles with different doping concentrations (0.015, 0.020 and 0.025 M) by precipitation method. XRD indicated the formation of single phase nanoparticles without any traces of impurity. Mg-doped ZnO nanoparticles were found to have diameters ranging from 60 to 90nm. The surface morphological analysis by SEM revealed granular and well dispersed ZnO nanoparticles while flake like structures having inhomogeneous distribution for Mg-doped ZnO nanoparticles. The optical properties were measured by using UV–Vis spectrophotometer and photoluminescence spectroscopy. Results showed that as the Mg concentration increases (0.015, 0.020 and 0.025 M) the optical absorption edge slightly shifts towards the longer wavelength region (i.e. band gap decreases) which may be attributed to the increase in the grain size.

Etacheri et al. [23] in 2012 synthesized Mg-doped ZnO ($Zn_{1-x}Mg_xO$; 0.02, 0.05, 0.10, and 0.20) nanoparticles via an oxalate coprecipitation method. XRD study showed single wurtzite phase for lower Mg-doping concentrations while a secondary phase (MgO) was found for higher doping concentrations. A significant compression of c-axis and reduction in crystallite sizes resulted from the Mg-doping in ZnO. XPS study also confirmed the substitution of Zn^{2+} by Mg^{2+} and crystallization of MgO secondary phase. Further, it revealed strengthening of Zn−O bond

due to the presence of secondary phase. PL study indicated a blue shift and decreasing intensity for the doped samples as compared to undoped ZnO. Mg-doped ZnO sample (x = 0.1) was found to show highest photocatalytic activity. The reason ascribed was the combined effect of better electron−hole separation, a wider band gap, and superior textural properties.

Wu et al. [24] in 2013 synthesized Mg-doped ZnO ($Zn_{1-x}Mg_xO$; $0 \leq x \leq 0.15$) nanoparticles through polyacrylamide polymer method. Mg doping causes decrease in lattice parameter *c* which suggested that Mg^{2+} was doped into ZnO lattice. The synthesized nanoparticles were found to be of diameter 70–85 nm. Doping of Mg^{2+} does not change the particle size and particle shape. With increasing the calcination temperature the crystallite size of the nanoparticles gets increased but no other phase was formed in the Mg doped ZnO. Mg doping shifted the absorption onset towards lower wavelengths (370–350 nm) with increase in Mg doping from 0 to 12.5%, indicating an increase of the band gap which was attributed to the influence of dopant ions.

Srivastava et al [25] in 2013 reported the possibility of non-magnetic doping induced magnetism, in Li doped SnO_2 nanoparticles which had been synthesized by solid state route at equilibrium. For a particular range of Li concentration, Li-doping induced magnetism in SnO_2 while for other Li concentrations, including pure SnO_2, the samples exhibit diamagnetism. The X-ray diffraction results provide the existence of single rutile phase. Results showed that 6% and 9% Li-doped compounds exhibit a magnetic phase at 3 K. However, other Li doped compounds, including SnO_2 are diamagnetic. The effect of annealing temperature on the magnetization in order to understand the observed magnetism had also been studied.

Jayanthi et al. [26] in 2009 synthesized ZnO nanocrystals doped with different groups of impurities, e.g., Li, Na, Cu, Pr and Mg were synthesized by solid-state reaction method. XRD characterize formation of mono phasic wurtzite structure with size variation between 33 nm and 143 nm. but change in lattice parameters and Zn–O bond length indicates incorporation of dopant ion in ZnO lattice. The dopant (lithium, sodium, copper, praseodymium, magnesium) has a significant influence on the morphology of ZnO. The morphology of ZnO nanocrystals exhibited striking dependence on type of dopant ion with the shape changing from nanorods, spherical to petal like particles.PL shows UV emission and negligible visible emission for Li, Na and Cu doped ZnO nanocrystals with peak positions coinciding with that of undoped ZnO. Undoped ZnO, Li and Na doped ZnO showed well-formed nanorods but Cu doped ZnO

nanorods are not so well formed and tends to form cluster. TEM analysis showed very well formed nanorods formation in Li and Na doped ZnO. HRTEM studies show distinct lattice fringes with SAED pattern indicating that individual nanoparticles form single crystals. Photoluminescence results have shown UV emission as well as visible emission related to defect levels created by Mg and Pr.

1.6 Zinc Oxide (ZnO)

ZnO is a wide band gap (3.37 eV) group II-VI based semiconductor. It possesses useful optical, chemical and electrical properties, and is nontoxic, inexpensive and chemically stable. ZnO has been extensively studied due to its intrinsic properties and potential applications in devices, such as field-effect transistors, solar cells, light emitting diode, photocatalyst etc [27]. After a lot of research it has been found that controlled synthesis of semiconductor nanostructures in terms of size and shape results in successful tuning of its properties. It has been found that morphology of nano-materials is also one of the key parameter that affects the properties of ZnO nano-structures. Till now, ZnO with different nanostructures, such as nanotetrapods, nanomultipods, nanosheets, nanotubes, nanowires and nanorods have been successfully synthesized. ZnO is transparent to visible light and can be made highly conductive by doping. It is also considered as a promising material for semiconductor device applications [28-30]. ZnO is available in large bulk single crystals and crystallizes in the wurtzite structure [31]. Lack of control in the electrical conductivity of ZnO has hindered its use in electronic devices [32]. ZnO crystals are always n-type, which has been considered as a matter of extensive debate and research. The qualities of ZnO single crystal substrates and epitaxial films have witnessed a significant improvement in last few decades. Thus, studies have been devoted by many research groups for using ZnO as an optoelectronic material and also that it can be used as an alternative for GaN. So investigations on its semiconductor properties in order to achieve p-type conductivity are of interest. First-principles calculations based on density functional theory (DFT) have a contribution towards understanding the role of native point defects and impurities on n-type conductivity of ZnO [33-35]. Other application areas of ZnO are biosensors, acoustic wave devices, gas sensors and solar cells. It is relatively easy to produce ZnO nanostructures, which possess good charge carrier transport properties and high crystalline quality. Inspite of the significant progress made in this area, still a number of important issues are needed to be resolved so that it can be used

commercially.

Due to high quantum efficiency possessed by ZnO, it is preferred over TiO_2 for the photocatalytic decomposition of organic pollutants [36−38]. In addition to this, ZnO can absorb and utilize larger fractions of solar spectrum compared to TiO_2. Photocatalytic activity of ZnO depends on various factors such as phase purity, surface area, crystallite size, nature of dopants, and method of preparation. Though ZnO is highly photocatalytically active, its band gap is not wide enough to utilize the high-energy solar radiations. This narrow band gap seriously deteriorates the photocatalytic activities of ZnO under sunlight irradiation, which has significant impacts on the commercial applications of these materials. In order to utilize solar radiations more effectively, the development of a wide band gap ZnO is necessary. Transition metal and anionic doping were employed previously for improving the photocatalytic activity of ZnO under sunlight irradiation [39].

Doping of Mg^{2+} ion in ZnO results in widening of the band gap while Cd^{2+}ions narrow the band gap. In both cases, alloys having hexagonal structure have been found to form. Also, a lot of interest in doping 3d transition metal ions in ZnO derives due to the potential applications in spintronics. Studies on bulk and nanocrystalline ZnO doped with 3d transition metal ions are primarily concerned with the magnetic properties.

1.7 Physical properties of ZnO

Physical properties of ZnO have been listed in Table 1.1, as shown below.

Table 1.1 Physical properties of ZnO

Lattice constants (T=300K)	a=0.32469 nm, c=0.52069 nm
Density	5,606 g/cm
Melting point	2248 K
Relative dielectric constant	8.66
Gap Energy	3.4 eV, direct
Intrinsic carrier concentration	<10 cm
Exciton Binding Energy	60 meV
Electron effective mass	0.24

Electron mobility	200 cm/V-s

1.8 Crystal structure of ZnO

Zinc oxide crystallizes in three forms: cubic zincblende, hexagonal wurtzite and cubic rocksalt. The wurtzite structure is most stable amongst them and hence is most common at ambient conditions. The zincblende structure can be stabilized via growth of ZnO on substrates having cubic lattice structure. The rocksalt NaCl-type structure is only observed at relatively high pressures ~10 G Pa.

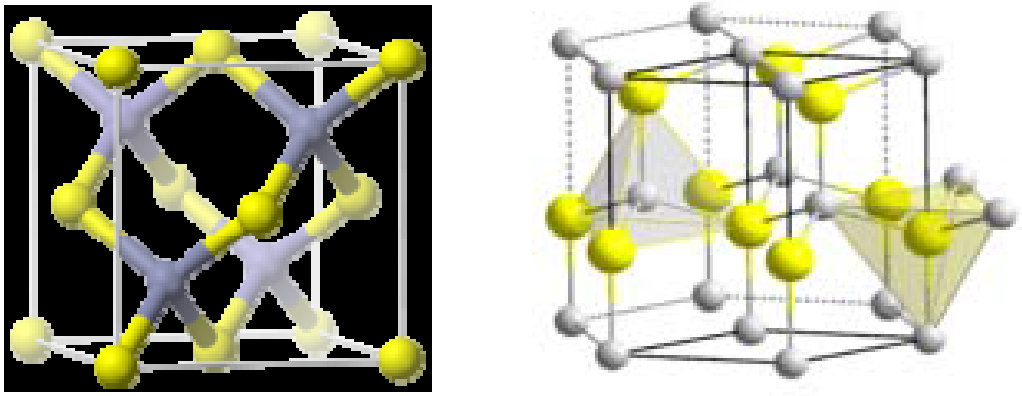

(a) (b)

Figure1.1 Crystal structures of ZnO (a) zincblende structure (b) wurtzite structure

The sphalerite structure (Figure 1.2 (a)), which is known as the zinc-blend structure, is based on a ccp array of bulky anions (O^{2-}) but cations (Zn^{2+}) occupy one type of tetrahedral hole, one haft the tetrahedral holes present in a close packed structure.

1.9 Sol- Gel Technique

The sol gel technique is based on hydrolysis of liquid precursors and formation of colloidal sols. The precursors are usually organosilicates yielding silicate sol-gel materials. However, the method is not restricted to the silicon compounds-for example compounds of zirconium, vanadium etc. can be used as precursors leading to materials possessing different physico-chemical properties.

The sol gel process is a wet chemical technique for the fabrication of materials starting either from a chemical solution or colloidal particles to produce an integrated network (gel). A sol stands for a stable dispersion of colloidal particles in a solvent. Typical precursors used are metal alkoxides, chlorides or nitrates, which undergo hydrolysis and polycondensation reactions to form a colloid, a system composed of solid particles dispersed in a solvent. The sol evolves towards forming an inorganic continuous network containing a liquid phase known as gel. The particles thus produced may be amorphous or crystalline. Sol gel is promising as well as a versatile method for synthesizing nanostructures of various morphologies, thin films, etc. of different materials. The growth in this method can be controlled via several factors. These factors include solvent, reaction temperature, precursors, catalysts, pH, additives and mechanical agitation. These factors can influence the kinetics of growth, the growth reaction, hydrolysis and condensation reactions that occur in the process. The solvent influences the growth kinetics and conformation of the precursors. The pH affects the hydrolysis and condensation reactions in the process. The pH also affects the stability of the sol which in turn also influences the particle size [16].Acidic conditions of the precursors favour the hydrolysis which forms fully or nearly fully hydrolyzed species before the condensation takes place. The basic conditions favour condensation reactions and therefore condensation begins before hydrolysis is complete. Thus these two conditions will give different species as the final product. The structure and the properties of the gel can be tailored by controlling the reaction rates of hydrolysis and condensation. The sol gel process is widely used for the synthesis of nanoparticles with binary or ternary compositions. The sol gel is a low temperature process and used to prepare pure, dense, stoichiometric and uniform particles.

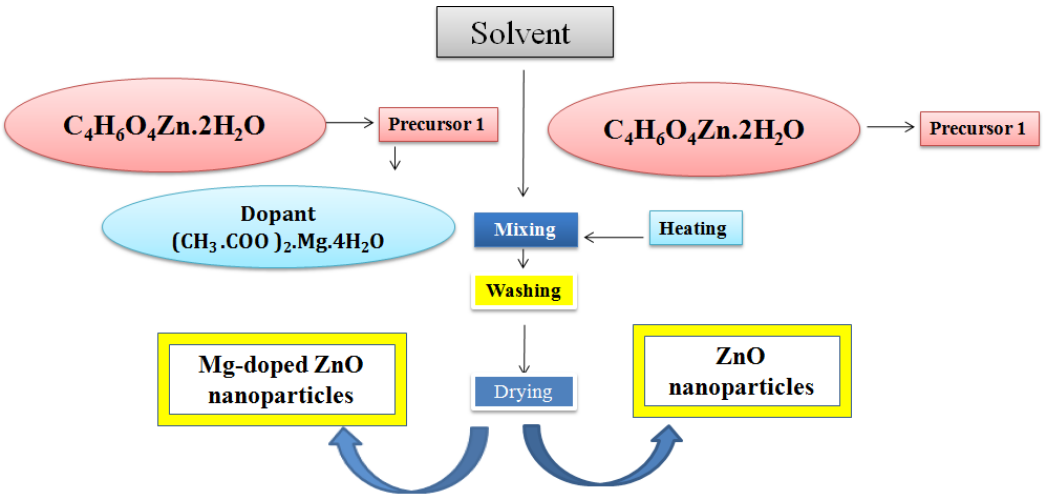

Fig1.3 Schematic of sol-gel technique

The schematic of the sol-gel technique employed for the synthesis of both undoped and Mg-doped ZnO nanoparticles has been shown in Figure 1.3. The following series of ZnO nanoparticles have been synthesized using above procedure;

- *Undoped , 5%, 10%, 15% and 20% Mg-doped ZnO nanoparticles*

The advantages of using sol-gel processing instead of high temperature processing methods are:

- low synthesis temperature
- high purity
- novel materials
- low capital costs

Chapter-2

Chapter-2

Characterization Techniques

2.1 X-Ray Diffraction (XRD)

X-ray diffraction is a non-destructive analytical methodology which can provide information about the chemical composition and crystallographic structure of natural and manufactured materials. It is used extensively for quality control of production, especially in research and development applications.

2.1.1 Working Principle

The interaction of the incident rays with the sample results in constructive interferences when Bragg's conditions is satisfied

$$2d\sin\theta = n\lambda$$

Where n = an integer, λ = wavelength of x-rays, d = inter planar spacing θ = diffraction angle

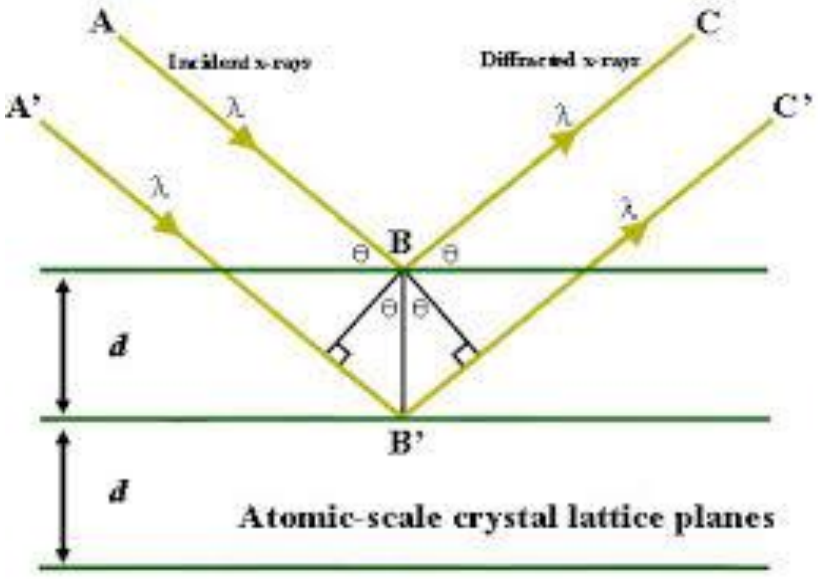

Figure 2.1 shows graphical representation of Bragg's law [40]

Bragg's law relates the wavelength of an electromagnetic radiation to the diffraction angle and the lattice spacing of a crystalline sample. Constructive interference and peak intensity occurs on satisfying the Bragg equation, when x-rays are incident on the sample. The diffracted x-rays are detected, processed and counted. It is possible to cover up all the possible diffraction directions of the lattice via scan through a range of 2θ degree due to the random orientation of the powdered material.

2.1.2 Instrumentation & Working

XRD consists of three basic elements i.e. an x- ray tube, a sample holder and an x- ray detector. x-rays are generated in a cathode ray tube. For this purpose, a heated filament is used to produce electrons, the electrons are accelerated towards a target by applying a voltage and these electrons bombard the target material.

Figure 2.2 Pictorial view of XRD

When electrons possess energy enough to eradicate the electrons in the inner shell of the target material then, characteristic x-ray spectra is formed. These spectra consists of several components, the most common being K_α and K_β. The specific wavelengths are characteristic of the target material. Filtering by foils is necessary to produce monochromatic x-rays required for diffraction. Approximately 1% of the total energy of the electron beam is converted into x-ray

radiation. In order to get a narrow beam of x-rays, the x-rays generated by the target material are allowed to pass through a collimator which consists of two sets of closely packed metal plates separated by a small gap. The collimator absorbs all the x-rays except the narrow beam that passes between the gaps.

2.1.3 Uses of XRD

- The identification of unknown crystalline materials.
- Identification of fine-grained minerals such as clays those are otherwise hard to determine optically.
- Determination of unit cell dimensions.
- Measurement of sample purity.

2.2 Transmission Electron Microscope (TEM)

The resolving ability of optical microscope is limited due to its wavelength. TEM was developed in order to obtain better magnification since electron's wavelength is exploited in it to obtain details of specimen to a much better level than the conventional optical microscopes. In TEM thin samples, which allow a fraction of the incident electron beam to go through the sample can be studied. It provides morphological and topographical information.

2.2.1 Principle

The operating principle of TEM is same as that of optical microscope except that electron is used instead of light. An accelerated beam of electrons impinges upon a sample; a rich variety of interactions takes place. In principle all these products of primary beam interaction can be used to derive information on the nature of the specimen. The highly accelerated electrons (few hundred keV) can cause scattering or backscattering elastically or inelastically, transmission of electrons, different signals such as x-rays, Auger electrons or light. The image in TEM is a result of transmitted electrons.

2.2.2 Instrumentation & Working

The illumination system comprises of gun and condenser lenses and their role is to take the electrons from the source and transfer them to the specimen. The electron beam is accelerated to energy in the range 20 - 1000 keV in the electron gun, then the electron beam passes though set of condenser lenses in order to produce a beam of electrons with a desired diameter (Figure 2.3). The illumination system can be operated in two principal modes: parallel beam and convergent beam. The first mode is used primarily for TEM imaging and selected area electron diffraction (SAED). In TEM, when a beam of electrons passes through specimen (ultra thin) it interacts with it as the beam passes thereby, causing the above mentioned various interactions.

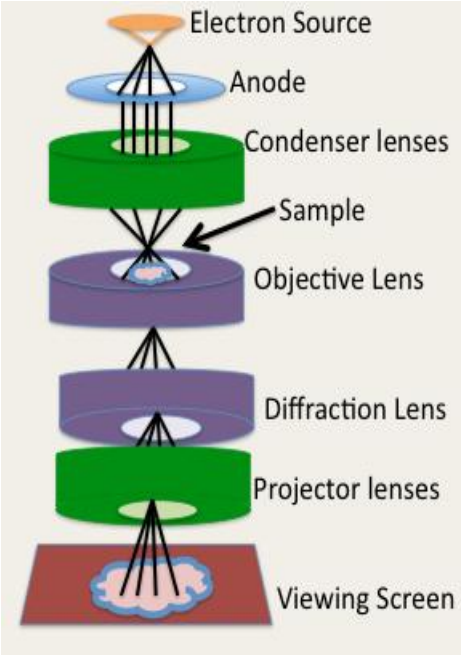

Figure 2.3 Schematic illustrating TEM [41]

An image is formed on interaction of transmitted electrons through the sample; the image is magnified and then, focused onto an imaging device, such as fluorescent screen, photographic film, or a sensor such as CCD camera. At smaller magnifications due to the thickness and composition of the material, the absorption of electrons in the material becomes responsible for

contrast of TEM image but at higher magnifications, expert analysis of observed images is required because complex wave interactions vary the intensity of the image.

2.2.3 Uses of TEM

TEM has a wide-range of applications in a variety of scientific, education, research and industrial fields. It is used in various applications in different field like in cancer research, semiconductor research, materials science, pollution and nanotechnology.

2.3 Energy Dispersive X-Ray Spectroscopy (EDS)

EDS is used mainly for elemental analysis and for chemical characterization of samples. All elements from atomic number 4 (Be) up to 92 (U) contained in the sample can be detected and analyzed simultaneously, but elements of low atomic number are difficult to detect by EDX.

2.3.1 Working Principle

In EDS, the incident electron beam excites an electron in an inner shell, causing its ejection and the formation of an electron hole in the electronic structure of the atom. An electron from a higher energy shell fills the hole, and the difference in energy between the higher energy shell and the lower energy is released as x-rays. The x-rays thus released are analyzed by means of an energy dispersive spectrometer. The amount of energy released by the transferring electron depends on which shell it is transferring from, as well as which shell it is transferring to. Furthermore, the atom of every element releases x-rays with unique amounts of energy during the transferring process. Thus, by measuring the amounts of energy present in the X-rays being released by a specimen during electron beam bombardment, the identity of the atom from which the X-ray was emitted can be established.

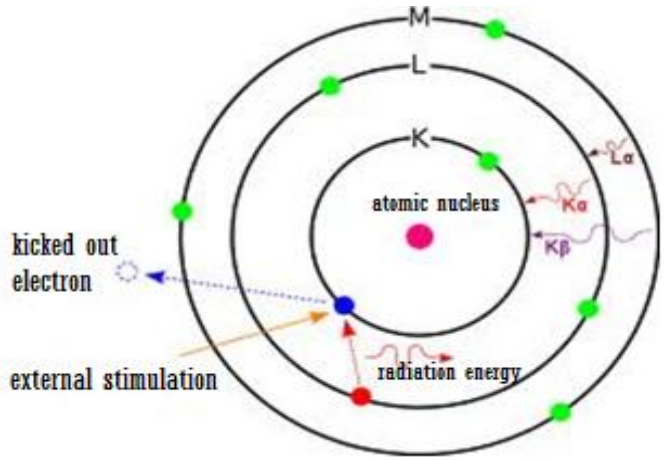

Figure 2.4 Working principle of EDS [42]

The emitted x-rays have energy which is characteristic of the parent element. Therefore, detection and measurement of the X ray energy helps in elemental analysis. EDX, therefore is a means of rapid qualitative and quantitative analysis of elemental composition of up to a depth of 1-2 microns.

2.3.2 Instrumentation & Working

There are four primary components of the EDX setup, beam source, x-ray detector, pulse processor and analyzer.

Figure2.5 Pictorial view of EDS [43]

Since EDX systems are mostly used with SEM, the SEM is equipped with a cathode as energy source and magnetic lenses to create and focus a beam of electrons. For the elemental analysis, a detector is used in SEM to convert x- ray energy into voltage signals and this information is sent

to a pulse processor which measures the signals and passes them onto an analyzer for data display and analysis.

2.3.3 Uses of EDS

Qualitative Analysis: The qualitative analysis is to determine the presence of an element in the sample. For this, its x-ray energy values from the EDX spectrum are compared with known characteristic x-ray energy value that corresponds to the atomic number of the elements present in the sample. The minimum detection limits vary from approximately 0.1 to a few atom.

Quantitative Analysis: The quantitative analysis is based on computing the relative x-ray counts at the characteristic energy levels for the sample constituents. Semi quantitative results are then readily available by using mathematical corrections based on the analysis parameters and the sample composition. Greater accuracy can be obtained using known standards with similar structure and composition to that of the unknown sample.

EDS has been widely used to determine the compositions of particles, contamination and thin film layers in wafer fabrication. The relative concentrations in weight, oxide, or atomic formula percentages can be obtained from the EDX spectra. Modern Detector allows for rapid analysis and concentration analysis in less than a minute. An EDX can be used in various fields like environmental testing, materials identification, home inspection metallography etc.

2.4 Photoluminescence Spectroscopy (PL)

It is a powerful technique for investigating the electronic structure of both intrinsic and extrinsic semiconducting nanomaterials. It concerns monitoring the light emitted from atoms or molecules after they have absorbed photons. PL Spectroscopy is suitable for the characterization of both organic and inorganic materials and the samples can be either in solid, liquid or gaseous forms.

2.4.1 Working Principle

When atoms or molecules are excited by an outside energy source such as light or heat, then electrons get excited to higher energy states. When the excited electrons return to their ground

state, they release the excess energy in the form of photons. Due to atomic structure difference, the various substances will emit photons of different wavelengths that can be measured and analyzed.

2.4.2 Instrumentation & Working

The system consists of a light source, a set of monochromators at excitation and emission stage, a sample stage and a detector as shown in Figure 2.6. Various types of light sources can be used as excitation sources, including lasers ,light emitting diodes and lamps, xenon arcs and mercury vapor lamps. Monochromator filters the light beam and selects a light of single wavelength for the excitation of the sample.

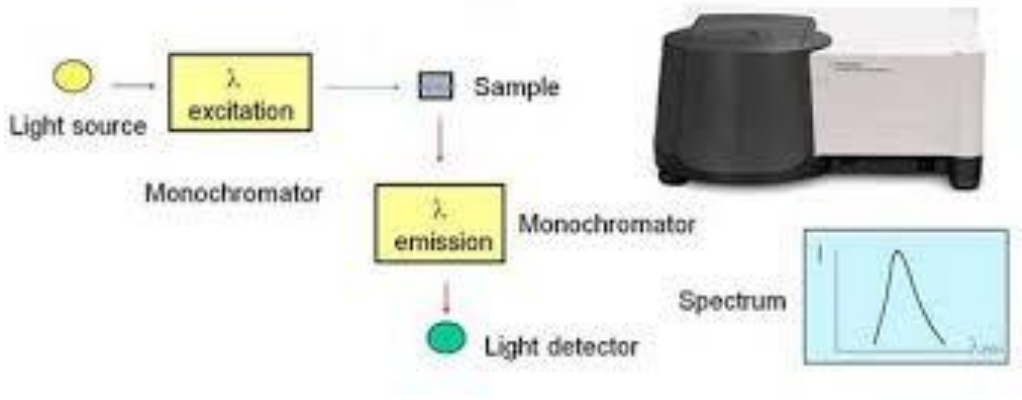

Figure 2.6 PL spectroscopy set up [44]

The light passes through the sample that emits light in all direction which is then passed through an emission monochromator and is collected by a detector. The signal is amplified using a photomultiplier and creates a voltage that is proportional to the measured emitted intensity. The excitation and emission monochromators thus, variable band pass filters. A second reference beam is attenuated and compared with the beam from the sample. The detector analyses it and provide signals to a CRT.

2.4.3 Uses of PL

- Determination of Band Gap

The radiative transition in semiconductors occurs between states in conduction and valence bands. These transitions are thus, used for the determination of the energy band gap of semiconductor.

- Detection of Impurity Levels and Defects

The radiative transitions also involve localized defect levels in semiconductors. PL energy associated with these levels can be used to identify specific defects. Further, PL intensity can be used to obtain their concentration.

- Recombination Mechanisms

The recombination mechanism involves both the radiative and non radiative processes. The dominant recombination process determines the PL intensity and its dependence on the level of photo excitation and room temperature. Therefore, the analysis of PL helps to understand the underlying physics of their recombination mechanism,

2.5 Electron Spin Resonance Spectroscopy (ESR)

ESR spectroscopy is a technique employed for measuring and interpreting the energy difference between atomic or molecular states. According to Plank's law, electromagnetic radiation will be absorbed if, $\Delta E = h\nu$, where ΔE is the difference in energy of the two states, *h* is Plank's constant and *v* is the frequency of the radiation. The energy thus absorbed causes a transition of electron from the lower to higher energy state. In this, frequency of the radiation used is held constant while varying the magnetic field. This results in an absorption spectrum.

2.5.1 Working Principle

EPR spectroscopy is based on the spin of an electron and magnetic moment associated with it. Electron when placed in the applied magnetic field, *Bo*, then there can be two possible spin of electrons, one with higher energy and one with lower energy. The cause of energy difference is Zeeman effect. The lower energy state is going to occur when the magnetic moment of the electron (μ) is aligned with the magnetic field direction while a higher energy state exists when alignment of μ is against the magnetic field. The two states are labeled by the projection of the electron spin, *MS*, on the direction of the magnetic field, where $M_S = -1/2$ is the parallel state, and $M_S = +1/2$ is the antiparallel state as shown in Figure 2.7.

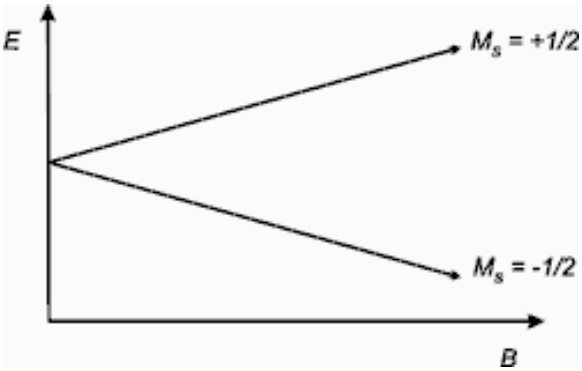

Figure 2.7 Schematic representation of electron spin in magnetic field

Hence, a molecule having one unpaired electron in magnetic field, the energy states of the electron are defined as follows

$$E = g\mu_B Bo M_S = \pm 1/2 g\mu_B Bo$$

where, g is the proportionality constant (or g-factor), μ_B is Bohr magneton, Bo is applied magnetic field, and M_S is electron spin quantum number. Two noticeable factors can be summarized from the above equation. First, two spin states possess same energy when no magnetic field is and second is the that there is linear increase in energy difference between the two spin states with increasing magnetic field strength.

2.5.2 Instrumentation & Working

The sample is placed in the resonator which is positioned between two electromagnets as shown in Figure 2.8. The microwave frequency is produced using klystron. Generally, microwave frequency is kept constant and applied magnetic field is varied. The condition where the magnetic field and the microwave frequency are "just right" to produce an EPR resonance (or absorption) is known as the resonance condition is detected by the spectrometer

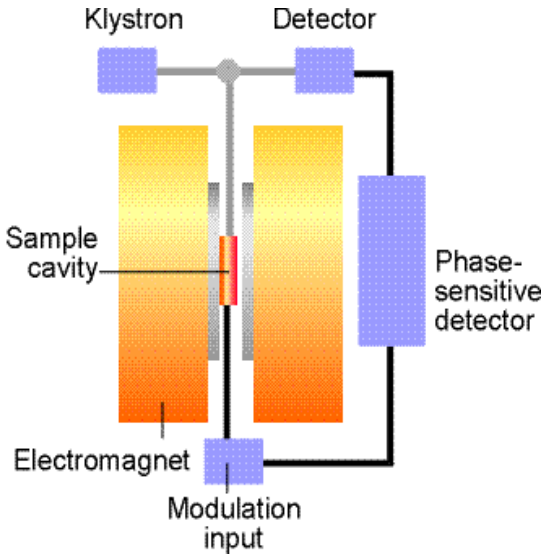

Figure 2.7 Schematic illustration of ESR spectrometer [45]

The most of EPR spectrometers are in the range of 8-10 GHz (X-band), though there are spectrometers which work at lower and higher fields: 1-2 GHz (L-band) and 2-4 GHz (S-band), 35 GHz (Q-band) and 95 GHz (W-band).

2.5.3 Uses of ESR

ESR spectroscopy is a direct and non-destructive technique for the detection of paramagnetic species that consists of one or more unpaired electrons. It has been widely used in a number of research fields such as physics, chemistry, biology and material and food science.

2.6 Vibrating Sample Magnetometer (VSM)

It is a scientific instrument that is used widespread for magnetic measurements. It has been designed by S. Foner, after its invention there have been many modification and improvement. Presently, it is a standard research instrument for magnetic measurement in many research laboratories.

2.6.1 Working Principle

VSM is based on Faraday's law of electromagnetic induction which states that change in magnetic flux will produce electric field.

2.6.2 Instrumentation & Working

In this technique, the magnetic specimen is vibrated with a certain frequency and amplitude employing a vibrator as shown in Figure 2.9. At the same time a static magnetic field is applied to magnetize the sample. Now, a set of pick up coils are kept near the sample to pick up the signal voltage induced in the coils due to the change in the magnetic flux linked, caused by the vibration of the magnetized sample. The signal has the same frequency of vibration and its amplitude will be proportional to the magnetic moment, amplitude, and relative position with respect to the pick-up coils system.

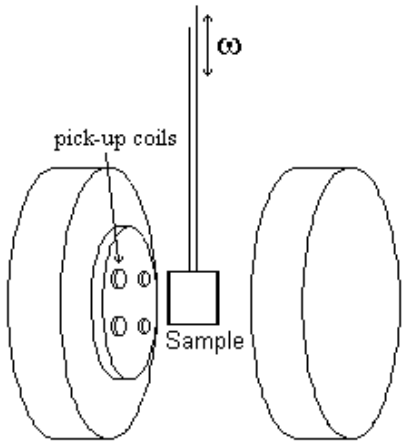

Figure2.8 Schematic illustration of VSM

The sample is placed in a small sample holder which is located in the middle of the electromagnet as shown in the Figure 2.9. The sample vibrates along the Z axis which is perpendicular to the applied magnetic field. The induced signal in the pick-up coil system is fed to a differential amplifier. The output of the differential amplifier is then passed into a tuned amplifier and an internal lock-in amplifier. The output is a DC signal which is directly proportional to the magnetic moment of the sample under investigation. Figure 2.10 shows the pictorial view of VSM.

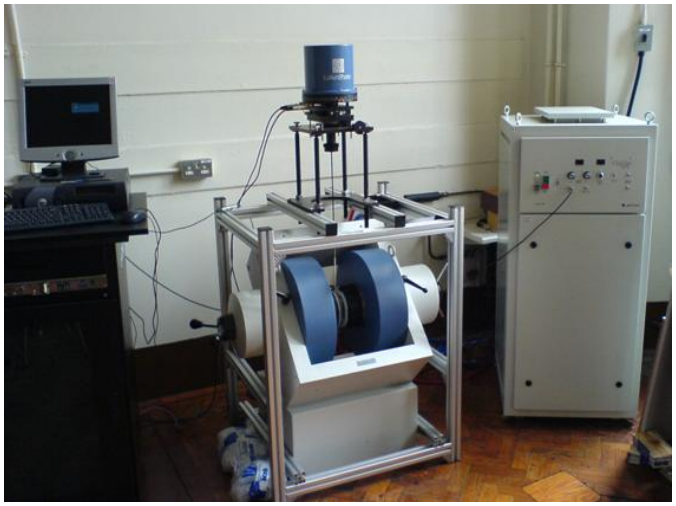

Figure 2.9. VSM Set-Up

2.6.3 Uses of VSM

VSM can be used to measure the DC magnetic moment as a function of magnetic field, temperature, time and angle. So, accordingly susceptibility and magnetization studies can be carried out. The measurements that can be performed with it includes: hysteresis curves, susceptibility or saturation magnetization as a function of temperature, magnetization curves vs angle (anisotropy) and time.

Chapter-3

Chapter-3

Results & Discussions

3.1 Structural analysis

Figure 3.1 shows XRD patterns of undoped and Mg-doped ZnO nanoparticles. All the diffraction peaks can be indexed to hexagonal structure (wurtzite phase) of ZnO (JCPDS card no. 75-0576). No additional peak related to any extra phase of Mg has been observed in XRD patterns, indicating the purity of synthesized nanoparticles. However, with increasing Mg-doping concentration, the peak shifted towards higher diffraction angle (Figure 1(b)). The observed peak shift can be attributed to smaller ionic radii of Mg^{2+}(0.57Å) as compared to Zn^{2+} (0.60 Å).

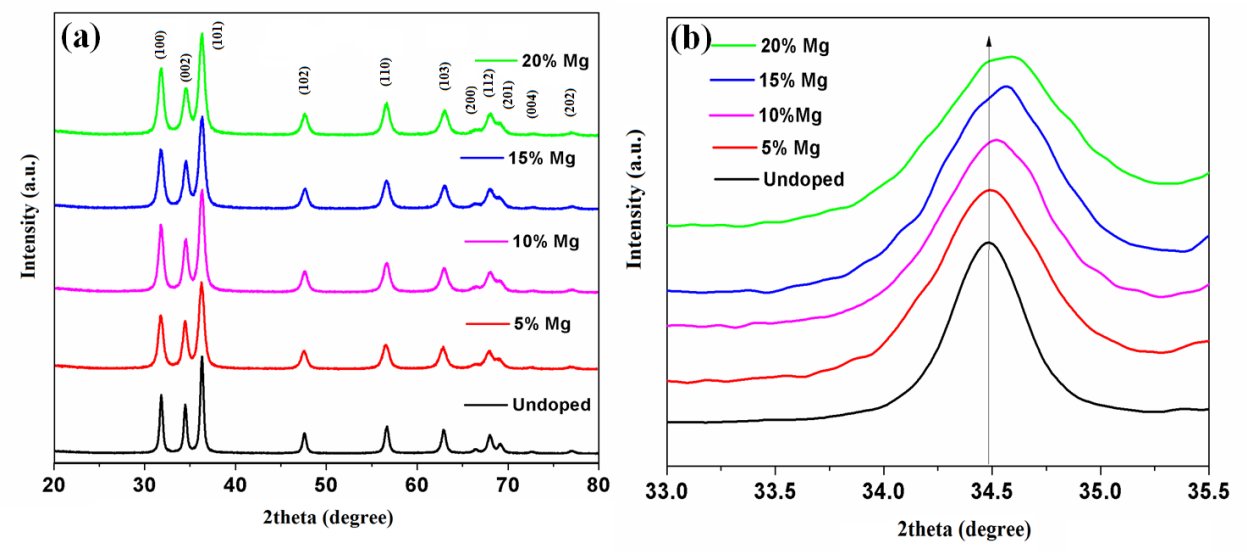

Figure 3.1(a) XRD pattern of undoped and Mg-doped ZnO nanoparticles and (b) expanded view at around ~ 2θ from 33-35.5º

The crystallite size has been calculated using the Debye-Scherrer equation [23]

$$D = \frac{0.9\,\lambda}{\beta\, Cos\theta} \qquad (1)$$

where D = crystallite size, λ = wavelength of X-ray used, β = full line width at the half-maximum height of the main intensity peak, and θ = Bragg angle.

The lattice parameters a and c have been calculated by using the formula [23]

$$\frac{1}{d^2} = \frac{4}{3}\left(\frac{h^2+k^2+l^2}{a^2}\right) + \frac{l^2}{c^2} \qquad (2)$$

The variation of crystallite size, interplanar spacing and lattice parameters has been shown in the Table 3.1. The lattice parameters have been found to be decreasing with the increase in doping content.

Table 3.1 Structural and lattice parameters of undoped, 5, 10, 15 and 20% Mg-doped ZnO nanoparticles.

Sample	c (Å)	a (Å)	Crystallite size (nm)	Interplanar spacing (Å)
Undoped	5.1974	3.1827	19.308	2.5987
5% Mg	5.1956	3.1816	12.348	2.5978
10% Mg	5.1850	3.1751	13.101	2.5925
15% Mg	5.1850	3.1751	11.797	2.5925
20% Mg	5.1824	3.1735	11.996	2.5912

3.2 Morphological and elemental analysis

The morphological analysis has been carried out using TEM. The samples were dispersed in ethanol and ultrasonicated for 30 min before taking TEM image. It has been observed that particle possesses almost spherical morphology having average particle size of 15 nm. Its corresponding HRTEM image (Figure 3.2(b)) indicates the presence of sharp lattice fringes having lattice spacing ~ 1.25 Å. It corresponds to d spacing of (202) crystal plane of wurtzite hexagonal ZnO (as revealed by XRD).

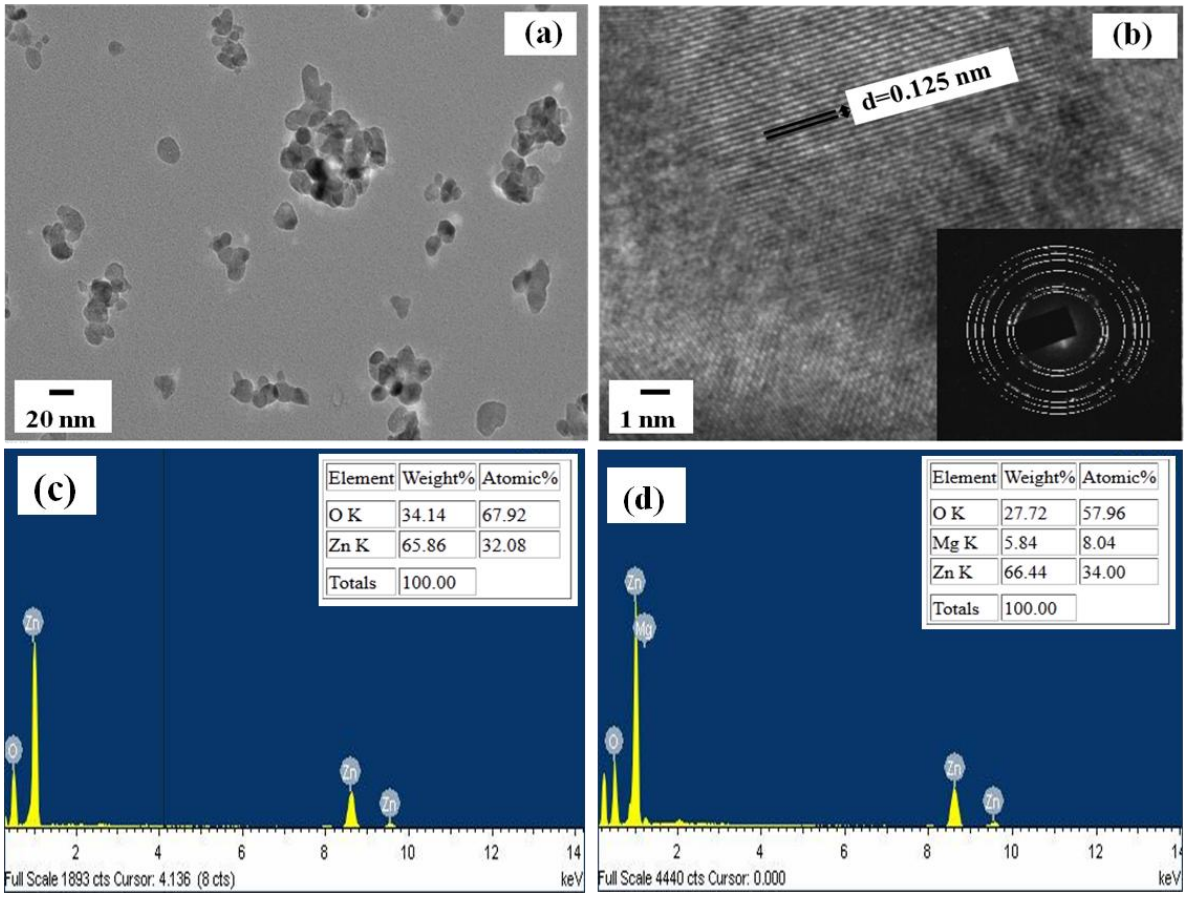

Figure 3. 2 (a) TEM image, (b) corresponding HRTEM and SAED image (inset) of 10% Mg-doped ZnO nanoparticles, EDS pattern of (c) undoped and (d) 10% Mg-doped ZnO nanoparticles

The inset shows its corresponding SAED pattern. It illustrates the sharp diffraction rings which indicate that highly crystalline and well developed nanoparticles. Figure 3.2(c) and (d) shows the EDS pattern of undoped and 10% Mg-doped ZnO nanoparticles. EDS spectra show the presence of Zn, O and Mg in the synthesized nanoparticles without any other contaminant. All the elements have been found to be in their stoichiometric ratio.

3.3 PL Spectroscopy Analysis

The room temperature PL spectra have been recorded at excitation wavelength of 350 nm, as shown in Figure 3.3. A sharp UV emission band has been observed for undoped ZnO nanoparticles at 389 nm. This is corresponding to the near band edge emission of ZnO [46].

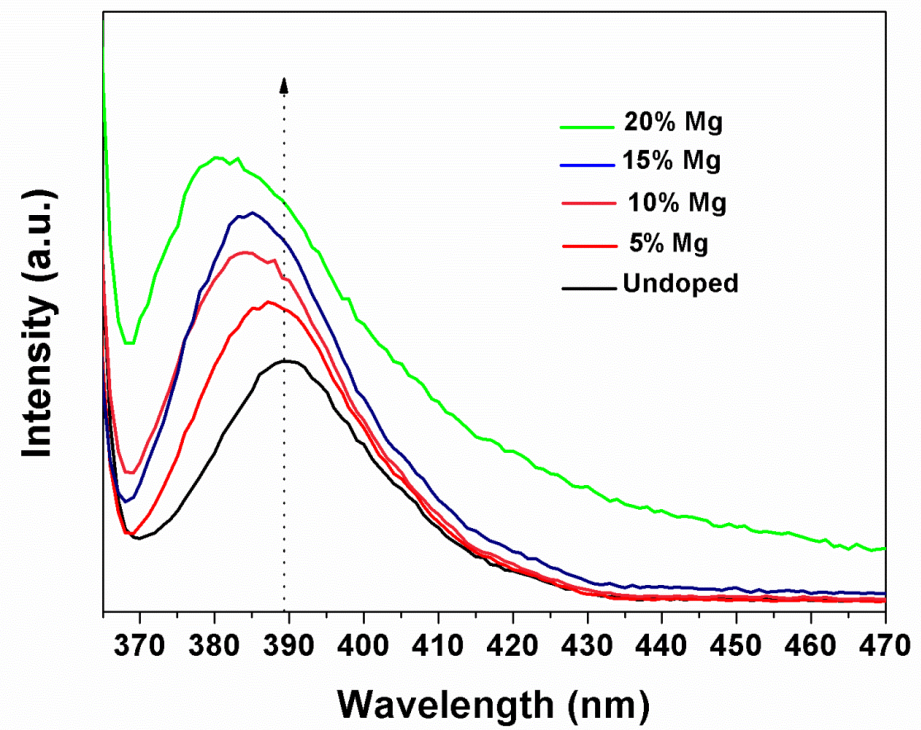

Figure 3.3 PL spectra of the undoped and Mg-doped ZnO nanoparticles

It has been observed that increasing Mg-doping concentration resulted in blue-shift of band gap. The band gap values have been found to be 3.17, 3.20, 3.22, 3.23, 3.26 eV for undoped, 5, 10, 15 and 20 % Mg-doped ZnO nanoparticles, respectively. This blue-shift in band gap cannot be ascribed to quantum confinement effect as Bohr exciton radius of ZnO is 1.8 - 2.0 nm. However, the observed blue-shift can be explained by the wider band gap of MgO (7.3 eV) as compared to ZnO (3.17 eV). The presence of blue-shifting and absence of defects related emission with increasing Mg-doping concentration have been observed in PL spectra (Figure 3.3). This indicates that Mg incorporation has not resulted in extra defects in host ZnO nanoparticles.

3.4 Electron Spin Resonance (ESR)

ESR measurements have been performed in order to know the origin and nature of observed ferromagnetism in Mg-doped ZnO nanoparticles. Figure 3.4 shows ESR spectroscopy of pure and Mg-doped ZnO nanoparticles.

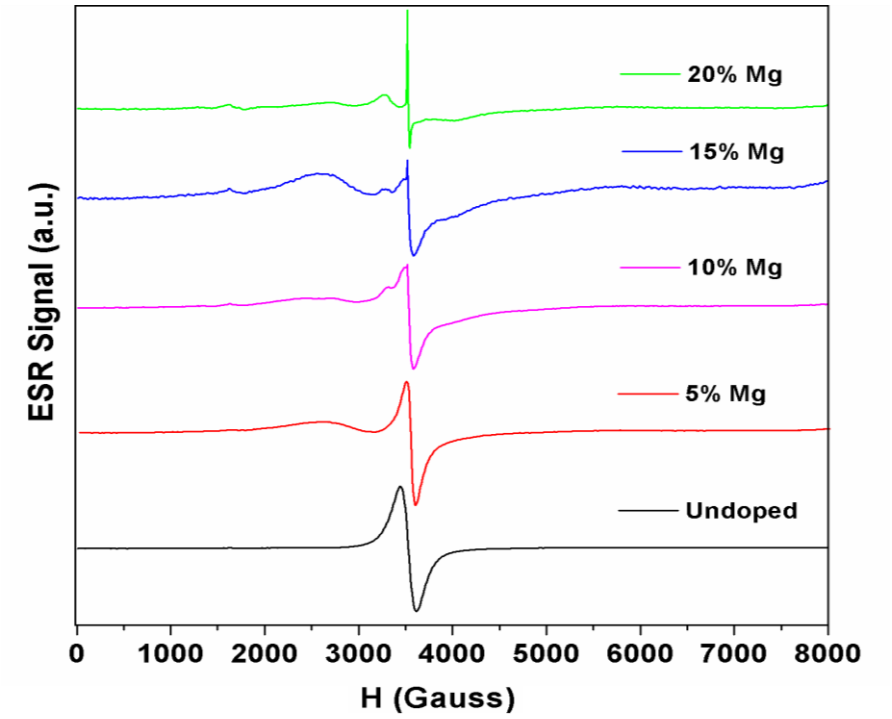

Figure 3.4 ESR Spectra of undoped and Mg doped ZnO nanoparticles

g- values have been calculated using following equation [47]

$$g = \frac{h\ v}{\mu_B\ B}$$

where *h* is Planck s constant, *v* is the microwave frequency and μ_B is the Bohr magneton.

The *g*-values have been found to be ~ 1.99 for undoped and Mg-doped ZnO nanoparticles. A broad resonance signal has been observed for undoped ZnO nanoparticles. Such resonance signal has been well reported in the literature which could be attributed to the electrons trapped in oxygen vacancy [47]. It has been observed from Figure 3.4 that with increase in the doping concentration, the resonance signal decreases. Generally, ZnO forms oxygen vacancies due to low formation energy (3.8 eV) as compared to Mg oxide (9.8 eV) [47]. Also, oxygen vacancies act as donor in ZnO. Mg-doping due to high formation energy attributes to decrease in oxygen vacancies leading to reduction in electron concentration in present work.

3.5 Vibrating Sample Magnetometer (VSM)

The magnetization versus applied magnetic field (M-H) measurements has been performed by using VSM, at room temperature. Fig 3.5 shows M-H hysteresis curves of undoped and Mg-doped ZnO nanoparticles. Room temperature ferromagnetism has been observed for both undoped and Mg-doped ZnO nanoparticles. Further, decay in room temperature ferromagnetism has been observed with increasing Mg doping concentration (Figure 3.5).

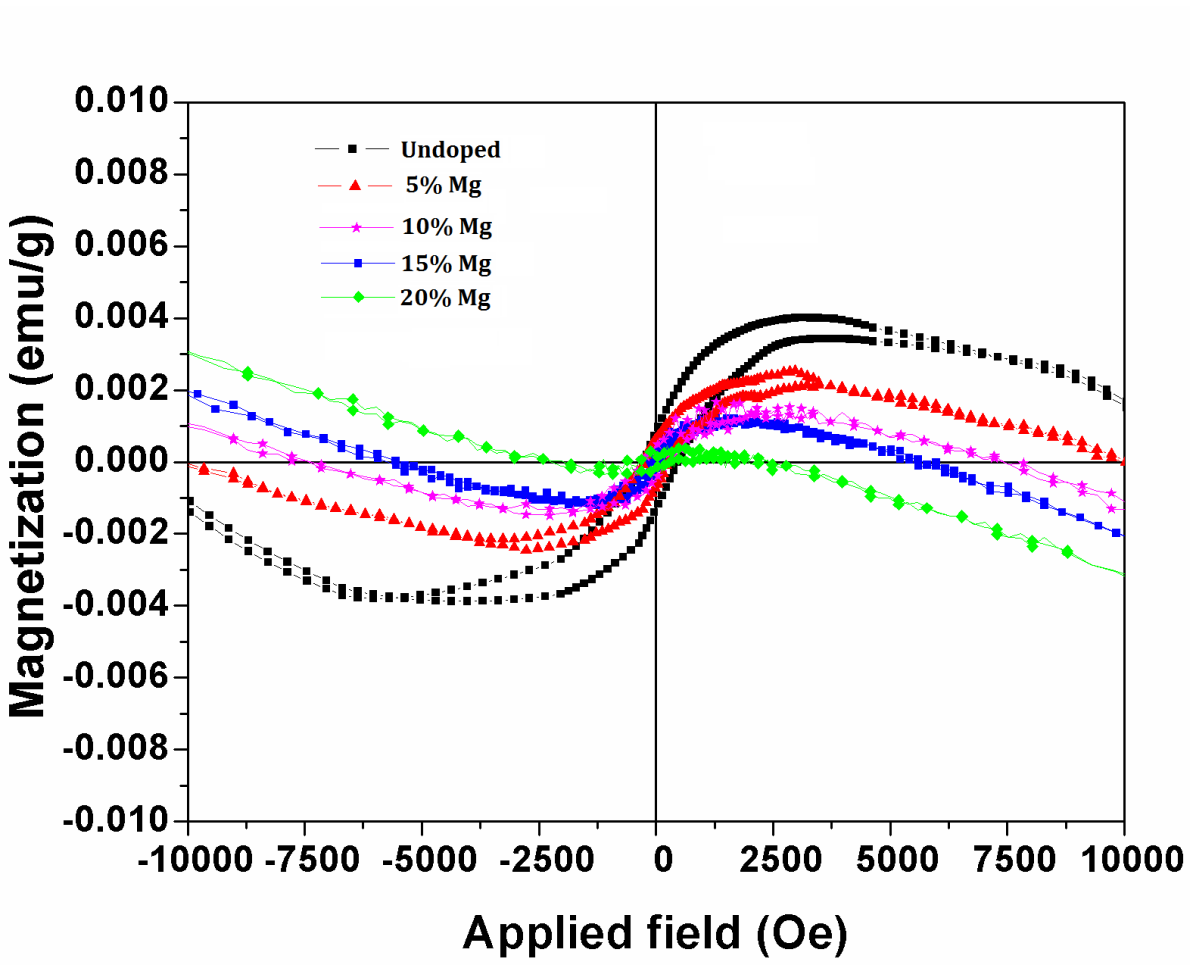

Figure 3. 5 M-H Loops for undoped, 5%, 10%, 15% and 20% Mg-doped ZnO nanoparticles

There are numerous reports in literature on the origin and observation of room temperature ferromagnetism in undoped ZnO nanoparticles [48]. The ferromagnetism can be attributed to various reasons such as charge transfer between capping agent and host nanoparticles, oxygen vacancies or defects. In present work no capping agent has been used, ruling out its contribution

in observed ferromagnetism. The origin of room temperature ferromagnetism can be linked to oxygen vacancies/defects in undoped ZnO nanoparticles. The exchange interactions between the trapped electrons in oxygen vacancy gives rise to resultant magnetization in undoped ZnO nanoparticles. This is in agreement with ESR analysis which indicates the presence of oxygen vacancies which have been found to decrease with increase in Mg-doping concentration. Accordingly room temperature ferromagnetism decreases with increase in doping concentration. Finally we conclude that the observed ferromagnetism is intrinsic in nature and does not comes from any impurity or extra phase.

Chapter-4

Chapter-4

Conclusions

4.1 Outcomes of Research Work

- The undoped and Mg-doped (5, 10, 15 and 20%) ZnO nanoparticles have been prepared using sol gel method.
- XRD analysis has been found to reveal the wurtzite phase having the hexagonal structure of nanoparticles. The decrease in crystalline size from 20 to 11 nm and the peak shifting towards higher diffraction angle has been observed with increase in Mg-doping concentration which thereby, confirms its substitution.
- TEM study has confirmed almost spherical nature of nanoparticles having average particle size of 15 nm. Clear lattice fringes and sharp diffraction rings have been observed in HRTEM and SAED patterns, respectively. These indicate that the synthesized nanoparticles are well crystalline in nature.
- EDS patterns have been found to show the presence of zinc, oxygen and magnesium without any other parasitic impurity. Hence, reveals the phase purity of the synthesized nanoparticles.
- The sharp near band edge emission has been observed in PL spectra. The blue-shift in band gap has been observed with increase in Mg doping concentration, owing to the wider band gap of MgO (7.3 eV) as compared to ZnO (3.17 eV).

- ESR resonance spectrum of undoped ZnO has been found to show the presence of oxygen vacancy/defects in host nanoparticles. ESR signal registers decrease with increase in Mg doping concentration, which indicates the decrease of oxygen vacancy/defects.
- Room temperature ferromagnetism behavior has been observed for all the synthesized nanoparticles. It has been observed that increasing Mg-doping concentration has resulted in decay of saturation magnetization value. The reason is attributed to the decreasing oxygen vacancy/defects with increasing Mg-doping, as revealed by ESR analysis.

4.2 Future Scope

- In order to see multiferroic behavior, the present work can be extended to other studies such as dielectric behaviour, polarization versus electric field (P-E measurement) and magneto electric coupling measurements etc.
- The influence of doping other non magnetic ions (B, Li, Al and N etc.) in host ZnO can also be investigated.

REFERENCES

1) S. Lindsay, "Introduction to nanoscience" Oxford University Press, UK (2010).
2) P. Boisseau, P. Houdy, M. Lahmani "Nanoscience: nanobiotechnology and nanobiology"c UK (2010).
3) H. E. Schaefer, "Nanoscience: The science of the small in physics, engineering, chemistry, biology and medicine" Springer, UK, (2010).
4) http://www.nanotechnology.com/docs/wtd015798.pdf
5) G. Cao, "Nanostructures & nanomaterials: Synthesis, properties and applications", Imperial college press, USA (2004).
6) D.C. Look, "Recent advances in ZnO materials and devices" *Material Science And Engineeering B*, **80**, 383-387 (2001).
7) R. Fiederling, M. Keim and G. Reusher., "Injection and detection of a spin polarized current in a light emitting diode", *Nature,* **402**, 787-790 (1999).
8) H. Saito, V. Zayets, S. Yamagata and K. Ando, "Optical properties and functions of dilute magnetic semiconductors" *Journal of Applied Physics,* **95**, 7175 (2004).
9) N. Ozaki, N. Nishizawa, K.-T. Nam, S. Kuroda and K. Takita, "Magnetic properties of MBE grown $Zn_{1-x}Cr_xTe$" *Physica Status Solidi C***, 1**, 957-960 (2004).
10) Y. Liu and L. Zhang, "Introduction to dilute magnetic semiconductors", *Progress in Physics,* **14**, 83-85 (1994).
11) I. Sieber, N. Wanderkaa, I. Urbanb, I. Do Erfelb, E. Schierhornb, F. Fenskea and W. Fuhs," Electron microscopic characterization of reactively sputtered ZnO films with different Al-doping levels," *Thin Solid Films,* **330**, 108-113 (1998).
12) Y. W. Ma, J. B. Yi, J. Ding, L. H. Van, H. T. Zhang and C. M. Ng "Inducing ferromagnetism in ZnO through doping of nonmagnetic elements" *Applied Physics Letters*, **93**, 042514 (2008)
13) X. Qiu, Liping Li, Jing Zheng, Junjie Liu, Xuefei Sun and Guangshe Li, **"**Origin of the Enhanced Photocatalytic Activities of Semiconductors: A Case Study of ZnO Doped with Mg^{2+}" *Journal of Physical Chemistry C***, 112**, 12242–12248 (2008)
14) S. Chawla, K. Jayanthi and R. K. Kotnala," Room-temperature ferromagnetism in Li-doped *p*-type luminescent ZnO nanorods" *Physical Review B***, 79**, 125204 (2009).

15) S. Chawla, K. Jayanthi and R. K. Kotnala, **"**High temperature carrier controlled ferromagnetism in alkali doped ZnO nanorods", *Journal of Applied Physics*, **106**, 113923 (2009).

16) D. Gao, Jing Zhang, Guijin Yang, Jinlin Zhang, Zhenhua Shi, Jing Qi, Zhaohui Zhang and Desheng Xue, "Ferromagnetism in ZnO Nanoparticles Induced by Doping of a Nonmagnetic Element: Al" *Journal of Physical Chemistry C***, 114**, 13477–13481 (2010)

17) H. Zhuang, J. Wang, H. Liu, J. Li and P. Xu," Structural and Optical Properties of ZnO Nanowires Doped with Magnesium" *Acta Physica Polonica A,* **119,** (2011).

18) B. Karthikeyan and T. Pandiyarajan "Simple room temperature synthesis and optical studies on Mg doped ZnO nanostructures" *Journal of Luminescence,* **130**, 2317–2321 (2010).

19) J.W. Park, D. H. Kim, S. H. Choi, M. Lee and D. Lim, "The Role of Carbon Doping in ZnO" *Journal of the Korean Physical Society*, **57**, 1482-1485 (2010).

20) J. Singh, M.S.L. Hudson, S.K. Pandey, R.S. Tiwari and O.N. Srivastava," Structural and hydrogenation studies of ZnO and Mg doped ZnO nanowires", *International Journal of Hydrogen Energy*, **37,** 3748-3754 (2012).

21) R. Viswanatha, T. G. Venkatesh, C.C. Vidyasagar and Y. Arthoba Nayaka, "Preparation and characterization of ZnO and Mg-ZnO nanoparticle" *Archives of Applied Science Research*, **4,** 480-486 (2012).

22) R. Viswanatha, Y. Arthoba Nayaka, C. C. Vidyasagar and T. G. Venkatesh, "Structural and optical properties of Mg doped ZnO nanoparticles" *Journal of Chemical and Pharmaceutical Research*, **4,** 1983-1989 (2012).

23) V. Etacheri, R. Roshan and V. Kumar, "Mg-Doped ZnO Nanoparticles for Efficient Sunlight-Driven Photocatalysis." *Applied Material Interfaces***, 4**, 2717−2725 (2012).

24) Y. Wu, J. Yun, L. Wang and X. Yang," Structure and optical properties of Mg-doped ZnO nanoparticles by polyacrylamide method." *Crystal Research Technology*, **48**, 145–152 (2013).

25) S. K. Srivastava, P. Lejay, A. H. Azzem and G. Bouzerar, "Non-magnetic doping induced magnetism in Li doped SnO_2 nanoparticles." *arXiv preprint arXiv*, **1302**,4869 (2013).

26) K. Jayanthi, S. Chawla, K. N. Sood, M. Chhibara and S. Singh, "Dopant induced morphology changes in ZnO nanocrystals."*Applied Surface Science*, **255**, 5869–5875 (2009).

27) Z. L. Wang, "Zinc oxide nanostructures: Growth, properties and Applications", *Journal of Physics: Condensed Matter*, **16**, R829 (2004).

28) D.C. Look, "Recent advances in ZnO materials and devices", *Material Science And Engineering* , **80**, 383-387 (2001).

29) I. Y. Alivov, C. Liu, A. Teke , M. A. Reshchikov , S. Dogan , V. Avrutin , Cho and H. Morkoc¸ "A comprehensive review of ZnO materials and devices, *Journal of Applied Physics*", **98**, 041301 (2005).

30) S. B. Ogale, "Thin films and heterostructures for oxide electronics",Springer, (2006).

31) D. C. Reynolds, D.C. Look and B. Jogai, "Optically pumped ultraviolet lasing from ZnO" Solid State Communications,**99**, 873-875 (1996).

32) C. Klingshirn, R. Hauschild, H. Priller, M. Decker, J. Zeller, H. Kalt, "ZnO rediscovered — once again*!?" Superlattices and Microstructures* **38**, 209–222, (2005).

33) C. G. Van de Walle, "Hydrogen as a Cause of Doping in Zinc Oxide" *Physical Review Letters*, **85**, 1012, (2000).

34) A. F. Kohan, G. Ceder, D.Morgan and C.G.Van de Walle, "First-principles study of native point defects in ZnO", *Physical Review* B, **61,** 15019 (2000).

35) C. G. Van de Walle "Defect analysis and engineering in ZnO" *Physical Review* B, **30,** 899-903 (2001).

36) C. A. K. Gouvea, F. Wypych, S. G. Moraes, N. Duran, N. Nagata, P. P. Zamora, **"**Semiconductor-assisted photocatalytic degradation of reactive dyes in aqueous solution", *Chemosphere*, **40**, 433-440 (2000).

37) S. K. Kansal, M. Singh, D. Sud, "Studies on photodegradation of two commercial dyes in aqueous phase using different photocatalysts" *Journal of Hazardous Materials*, **141**, 581-590 (2007).

38) M. Muruganandham, I.S. Chen and J.J. Wu, **"**Effect of temperature on the formation of macroporous ZnO bundles and its application in photocatalysis**"** *Journal of Hazardous Materials*, **172**, 700-706 (2009).

39) J. T. Luo, Y.C. Yang, X.Y. Zhu, G. Chen, G, F. Zeng and F.Pan, "Enhanced electromechanical response of Fe-doped ZnO films by modulating the chemical state and ionic size of the Fe dopant" Physical Review B, **82**, 14116 (2010),

40) http://serc.carleton.edu/research_education/geochemsheets/BraggsLaw.html

41) http://www.uni-ulm.de/elektronenmikroskopie/TEM_H2002.html

42) http://en.wikipedia.org/wiki/Energy-dispersive_X-ray_spectroscopy

43) http://www.iiti.ac.in/sic/index.php?q=eds

44) http://www.agilent.com/labs/features/2011_101_spectroscopy.html

45) http://web.nmsu.edu/~snsm/classes/chem435/Lab7/

46) W. Q. Peng, S. C. Qu, G. W. Cong, and Z. G. Wang**,** "Synthesis and temperature-dependent near-band-edge emission of chain-like Mg-doped ZnO nanoparticles" *Applied Physics Letters*, **88**, 101902 (2006).

47) P. K. Sharma, A. C. Pandey, G. Zolnierkiewicz, N. Guskos and C. Rudowicz, "Relationship between oxygen defects and the photoluminescence property of ZnO nanoparticles: A spectroscopic view" Journal of Applied Physics, **106**, 094314 (2009).

48) P. K. Sharma, R. K. Dutta, A. C. Pandey "Effect of iron doping concentration on magnetic properties of ZnO nanoparticles", *Journal of Magnetism and Magnetic Materials*, 321**,** 2587–2591 (2009).